Polyhedron 117 (2016) 437–444

Contents lists available at ScienceDirect

Polyhedron

journal homepage: www.elsevier.com/locate/poly

Chiral zinc(II) and cadmium(II) complexes with a dihydrophenanthroline ligand bearing (–)-α-pinene fragments: Synthesis, crystal structures and photophysical properties

Tatyana E. Kokina [a,b,*], Ludmila A. Glinskaya [a], Alexey V. Tkachev [b,c], Victor F. Plyusnin [b,d], Yuliya V. Tsoy [b], Irina Yu. Bagryanskaya [b,c], Evgene S. Vasilyev [c], Dmitriy A. Piryazev [a,b], Liliya A. Sheludyakova [a,b], Stanislav V. Larionov [a,b]

[a] Nikolaev Institute of Inorganic Chemistry, Siberian Branch of Russian Academy of Sciences, 3, Acad. Lavrentiev Ave., Novosibirsk 630090, Russia
[b] Novosibirsk State University, 2, Pirogov Str., 630090 Novosibirsk, Russia
[c] Vorozhtsov Novosibirsk Institute of Organic Chemistry, Siberian Branch of Russian Academy of Sciences, 9, Acad. Lavrentiev Ave., Novosibirsk 630090, Russia
[d] Institute of Chemical Kinetics and Combustion, Siberian Branch of Russian Academy of Sciences, 3, Institutskaya, Novosibirsk 630090, Russia

ARTICLE INFO

Article history:
Received 6 April 2016
Accepted 8 June 2016
Available online 17 June 2016

Keywords:
Chiral complexes
Pentacyclic heterocycle
Crystal structure
DFT-calculation
Photoluminescence

ABSTRACT

Mononuclear and dinuclear zinc(II) and cadmium(II) complexes, $[ZnLCl_2]$ (**1**) and $[Cd_2L_2Cl_4]$ (**2**), with a chiral pentacyclic dihydrophenanthroline ligand L bearing a natural monoterpene (–)-α-pinene fragment were synthesized. DFT calculations of the specific rotation [α] and an NMR study show that the molecules of ligand **L**, complex **1** and the monomeric form of complex **2** exist in $CDCl_3$ solutions with the *P*-helix conformation for the dihydrophenanthroline moiety. The dihydrophenanthroline fragments of **L** and mononuclear complex **1** also exists as a *P*-helix in the solid state, whereas the crystalline dinuclear complex **2** exists as an asymmetric dimer, $[Cd_2Cl_4L^PL^M]$, where L^P and L^M are the ligand with *P*-helix and *M*-helix conformations of the dihydrophenanthroline fragment respectively. Full sets of photophysical parameters for **L** and complexes **1** and **2** have been determined. Compounds **L**, **1** and **2** display blue luminescence (λ_{max} = 427, 405 and 415 nm in the solid state, respectively). The ligand **L** and complex **2** show moderate-to high quantum yields of 44% and 24%, respectively. The quantum yield for complex **1** is 6%. The emission lifetimes increase on going along the spectrum of luminescence, and in the deep red region, a rise of luminescence with times of 200–500 ps is observed. These processes can be explained by the migration of excitons and the capture of excitation by "defective" centers.

1. Introduction

The stereoselective synthesis of coordination compounds has attracted considerable interest over the past two decades [1–3]. Chiral coordination compounds are of special interest for asymmetric catalysis and metallosupramolecular chemistry [4–6]. In addition, chiral coordination compounds can demonstrate non-trivial physical properties, like circularly polarized luminescence, and often show various kinds of biological activity [7]. The use of optically pure ligands, especially natural products or their derivatives, is an effective method for the stereoselective synthesis of chiral coordination compounds [7–9]. Terpenes 'as is' are inactive ligands or demonstrate a weak coordination ability toward metal ions, whereas synthetic nitrogen-containing derivatives of natural terpenes are promising ligands for transition metals [10–12], especially in the case of the integration of the terpene moiety and azaheterocycles (pyrazoles, pyrazolinols, etc.) to give hybrid multidentate chiral ligands [13–17]. Chiral hybrids with the pinane moiety fused to a 2,2′-bipyridine backbone can form chiral luminescent metal complexes [18–20].

Luminescent zinc(II) and cadmium(II) complexes are of interest as promising fluorescent materials and sensors [21–32]. We have recently reported zinc(II) and cadmium(II) chloride complexes with an achiral pyridophenazine ligand prepared by functionalization of chiral pinopyridine [33]. Coordination of the ligand with zinc(II) and cadmium(II) ions leads to a spectacular increase in luminescence intensity, the mononuclear and dinuclear zinc(II) and cadmium(II) complexes showing bright photoluminescence both in the solid state and in solutions due to a considerable reduction of non-radiative rate constants k_{nr} in comparison with the free

* Corresponding author at: Nikolaev Institute of Inorganic Chemistry, Siberian Branch of Russian Academy of Sciences, 3, Acad. Lavrentiev Ave., Novosibirsk 630090, Russia.

http://dx.doi.org/10.1016/j.poly.2016.06.018
0277-5387/

ligand. The example mentioned demonstrates the use of a fused tetracyclic compound as a ligand showing a promising approach to metal complexes with intensive photoluminescence. Thus, the syntheses and spectroscopic study of new chiral luminescent zinc (II) and cadmium(II) complexes of pentacyclic nitrogen-containing fused terpene-based heterocycles are of great interest.

In this context we have endeavored to synthesize luminescent metal complexes with a new pentacyclic chiral ligand, (2*R*,4*R*,9*R*,11*R*)-3,3,10,10-tetramethyl-1,2,3,4,6,7,9,10,11,12-hexahydro-2,4,9,11-dimethanobenzo[*b*,*j*][1,10]phenanthroline (**L**) (Scheme 1), whose hybrid molecule contains two (−)-α-pinene moieties fused to an N,N-chelating dihydrophenanthroline core [34]. Luminescent zinc(II) and cadmium(II) complexes with a pentacyclic N-heterocycle containing two (−)-α-pinene fragments have not been previously described. We expected that the new chiral complexes would be good candidates for observing circularly polarized luminescence [35]. Here we describe (*i*) the synthesis of new zinc(II) and cadmium(II) complexes with the chiral ligand **L**, (*ii*) the X-ray single crystal structures of the ligand and the complexes, (*iii*) calculated (DFT) and experimental values of the specific rotation [α] for the free ligand and for the complexes, as well as NMR data demonstrating peculiarities of the conformational behavior of both the free ligand and the complexes (*iv*) detailed photophysical studies on the luminescence of all the compounds in both solution and the solid state.

2. Experimental

2.1. Reagents and methods

Reagent **L** was prepared by a technique reported in Ref. [34]. The following compounds were used for the synthesis of the complexes: $ZnCl_2$ and $CdCl_2{\cdot}2.5H_2O$ (pure for analysis), EtOH (rectified), and CH_2Cl_2 and *i*-PrOH (chemically pure). Elemental analysis was performed using an Euro EA 3000 analyzer. The molecular weight of complex **2** was determined on a KNAUER K-7000 vapor pressure osmometer in $CHCl_3$. The optical rotation angle was measured on a PolAAr 3005 instrument: **L** ($[\alpha]^{20}_{589}$-184, $[\alpha]^{20}_{546}$-224, $[\alpha]^{20}_{436}$-431, $[\alpha]^{20}_{405}$-559 (*c* 2.91, $CHCl_3$), $[\alpha]^{30}_{589}$-177, $[\alpha]^{30}_{546}$-221, $[\alpha]^{30}_{436}$-435, $[\alpha]^{30}_{405}$-600 (*c* 1.04, EtOH)); **1** ($[\alpha]^{26}_{589}$-170, $[\alpha]^{26}_{546}$-218, $[\alpha]^{26}_{436}$-520, $[\alpha]^{26}_{405}$-790 (*c* .191, $CHCl_3$)); **2** ($[\alpha]^{25}_{589}$-157, $[\alpha]^{25}_{546}$-195, $[\alpha]^{25}_{436}$-461, $[\alpha]^{25}_{405}$-692 (*c* 0.524, $CHCl_3$)). IR absorption spectra were recorded on SCIMITAR FTS 2000 and VERTEX-80 spectrophotometers in the range 4000–100 cm^{-1}. NMR spectra of solutions of the compounds in a $CDCl_3$-CCl_4 mixture (1:1 v/v, 5–20 mg/ml) were recorded at 300 K using a Bruker DRX-500 instrument (500.13 MHz for ^1H, 125.75 MHz for ^{13}C). NMR spectral data for the ligand **L** and complexes **1** and **2** are listed in Tables S1 and S2 (Supporting information).

Geometry optimization and optical activity calculations ([α]) were carried out using Density Functional Theory with the hybrid exchange–correlation functional B3LYP (6-31G* for **L** and for complex **1**, LanL2DZ [36] for complex **2**). All the calculations, except for the dimeric form of complex **2**, were carried out while maintaining C_2-symmetry. The X-ray crystallographic data were used as the starting coordinates in the geometry optimization of the dinuclear complex **2**. The solvent influence was taken into consideration using the Polarizable Continuum Model (PCM) [37]. All the calculations were carried out using the Dalton 2015.0 program [38,39]. The calculated values of the optical rotation are shown in Figs. 1, S1 and S2. Semi-empirical calculations were carried out using the ORCA program system [40]. Optimized geometries of the ligand **L** and complexes **1** and **2** were used in the estimation of $^1H^1H$ vicinal spin–spin coupling [41].

The excitation and luminescence spectra of the compounds in the solid state were detected using an FLS920 spectrofluorimeter (Edinburg Instruments) at room temperature. The solid samples for recording the luminescence spectra and kinetics were prepared by grinding the compounds to a powder between two quartz glasses. A thin layer of powder between glasses was placed at 45° to the excitation light beam. A xenon Xe900 lamp was employed as the excitation light source for the steady-state luminescence spectra. To record the kinetics, a diode EPLED-320 laser (λ_{ex} = 320 nm, pulse duration 0.6 ns) and a diode laser (λ_{ex} = 375 - nm, pulse duration 60 ps) were applied. The complicated luminescence kinetics were fitted by mono- and triexponential approximations using the FLS920 program or FAST program (Edinburg Instruments). Anthracene was used as a standard to calculate the quantum yields. The optical absorption spectra were recorded on an HP 8453 spectrophotometer (Agilent Technologies) with a diode line.

2.2. Synthesis of the complexes

2.2.1. Synthesis of $[ZnLCl_2]$ (**1**)

A solution of $ZnCl_2$ (0.020 g, 0.15 mmol) in *i*-PrOH (2 mL) was added dropwise to a stirred solution of L (0.037 g, 0.1 mmol) in a mixture of *i*-PrOH and CH_2Cl_2 (1:1 v/v, 4 mL). The solution was stirred and kept at room temperature. Small crystals formed when the volume of the solution became *ca.* 1–2 mL. The white precipitate

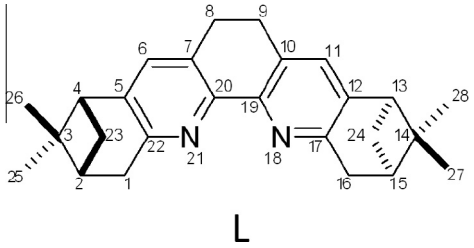

Scheme 1. The structure of the ligand L (atomic numbering is given for assignment of the NMR spectra).

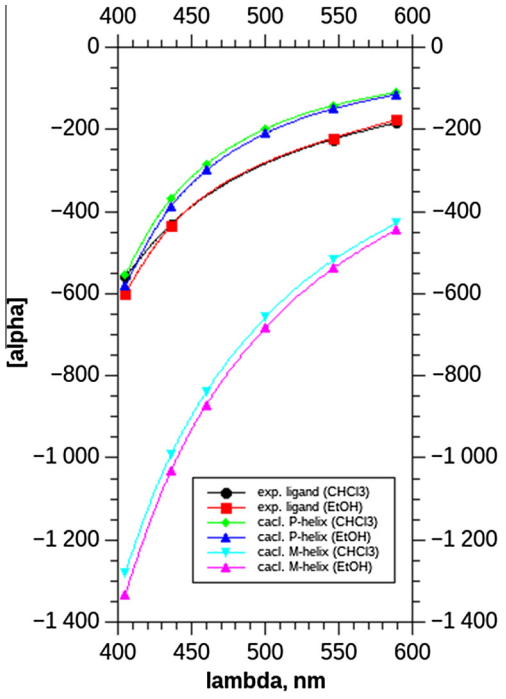

Fig. 1. DFT calculated and experimental values of [α] for compound **L**.

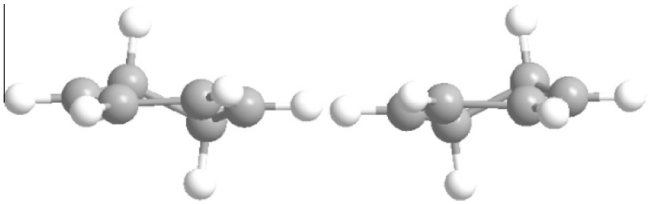

Scheme 2. Conformations of 1,3-cyclohexadiene.

was filtered off, washed with cold *i*-PrOH and dried *in vacuo* at room temperature. Yield 0.033 g (65%). *Anal.* Calc. for $C_{26}H_{30}Cl_2N_2Zn$ (506.8): C, 61.6; H, 6.0; N, 5.5. Found: C, 61.5; H, 5.8; N, 5.5%. Single crystals of complex **1** were grown by slow evaporation of a solution of this compound in an acetone-EtOH (1:1 v/v) mixture.

2.2.2. Synthesis of $[Cd_2L_2Cl_4]$ (**2**)

A solution of L (0.037 g, 0.1 mmol) in 3 mL of CH_2Cl_2 was added to a stirred solution of $CdCl_2 2.5H_2O$ (0.023 g, 0.1 mmol) in 3 mL of EtOH. The resulting solution was stirred and evaporated to a minimal volume (~1 mL). After that, the precipitated yellow residue was filtered off, washed with cold *i*-PrOH and dried *in vacuo* at room temperature. Yield 0.040 g (72%). *Anal.* Calc. for $C_{52}H_{60}Cl_4N_4Cd_2$ (1107.7): C, 56.4; H, 5.3; N, 5.1. Found: C, 56.0; H, 5.3; N, 5.0%. Molecular weight. Calc. for $C_{52}H_{60}Cl_4N_4Cd_2$:1107.7 and $C_{26}H_{30}N_2CdCl_2$: 553.8. Found in $CHCl_3$: 552 ± 5. Single crystals of complex **2** were grown by slow evaporation of the mother liquor.

2.3. X-ray crystallography

Single crystals of **L** were prepared by slow evaporation of a solution of this compound in a benzene-ethylacetate mixture. X-ray analysis for **L** was performed on a KAPPA APEX II (Bruker) diffractometer with a two-axis CCD detector using ω-φ scans. The unit cell parameters and intensities of reflections were measured at 298 K for **1** and 150 K for **2** on a Bruker X8 Apex CCD diffractometer equipped with a two-axis detector by standard techniques (Mo K radiation, λ = 0.71073 Å, graphite monochromator). Crystallographic characteristics, experimental data and structure refinements are listed in Table S3. Calculations on the structure of **L** were conducted with PLATON [42] and MERCURY [43] programs. The structures of complexes **1** and **2** were solved by direct methods and refined by the full-matrix least-squares method on F^2 in an anisotropic approximation for non-hydrogen atoms using the SHELXL-97 program package [44,45]. The H atoms on the C atoms were located geometrically and refined using a riding model. Selected interatomic distances and bond angles are given in Tables S4 and S5 (Supporting information). Simulated X-ray diffraction patterns of the compounds agree well with the experimental patterns.

3. Results and discussion

3.1. Synthetic aspects

Complexes **1** and **2** were synthesized by reacting Zn(II) and Cd (II) chloride with **L** in *i*-PrOH-CH_2Cl_2 and EtOH-CH_2Cl_2 mixtures respectively. A zinc-to-ligand molar ratio of 1.5:1 was applied for the synthesis of **1**. The complex **2** was prepared using a 1:1 cadmium-to-ligand molar ratio. According to the data of vapor-phase osmometry the dinuclear complex **2** dissociates into $CdLCl_2$ monomers in $CHCl_3$ solution.

3.2. DTF-calculation and NMR study

Quantum chemical calculations were used to predict the optical rotation ([α]) and to estimate the NMR parameters (some spin–spin couplings) of the levorotatory starting ligand **L**, complex **1** and the monomeric form of complex **2** in solution.

The 1,3-cyclohexadiene moiety of molecule **L** can exists in two C_2-symmetric conformations (Scheme 2).

Combining this 1,3-cyclohexadiene moiety with two pyridine rings results in two conformations of the dihydrophenanthroline fragment, with the *P*- or *M*-helicity: the sign (+) of the dihedral angle N–C–C–N corresponds to the *P*-helicity, while the sign (−) corresponds to the *M*-helicity. The two forms of the dihydrophenanthroline fragment lead to two diastereomeric conformations of the starting ligand **L** (Scheme 3).

Both semi-empirical quantum chemical calculations (AM1, MNDO, PM3) and DFT calculations (B3LYP/3-21G, B3LYP/6-311G, B3LYP/6-31G(d), B3LYP/6-31G(d,p) B3LYP/6-31G* without a solvent or in solution) predict that the M-helix and P-helix are isoenergetic. Calculations for 1,3-cyclohexadiene and related structures [46] allowed us to estimate the inversion barrier for these conformations: it appeared to be less than 4 kcal/mol. Thus, the conformation exchange should be fast on the NMR timescale, resulting in narrow averaged lines in the NMR spectra.

The two conformations of the dihydrophenanthroline fragments are transformed one to another by a ring inversion of the 1,3-cyclohexadiene moiety, so the equatorial and the axial hydrogen atoms of the dimethylene linkage $-CH_2CH_2-$ are in exchange. In the ^{1}H NMR spectrum, the $-CH_2CH_2-$ fragment appears at δ 2.84 ppm as a spin system of the AA'BB' type with the following parameters: $\Delta\delta_{AB}$ = 27.5 Hz, $J_{AB} = J_{A'B'}$ = -15.1 Hz, $J_{AA'}$ = 10.6 Hz, $J_{AB'} = J_{A'B}$ = 6.1 Hz, $J_{BB'}$ = 7.3 Hz (see Table S1). The calculated 1,2-diaxial vicinal coupling ($\varphi_{H-C-C-H}$ = 171°, $^3J_{H-H} \approx 12$ Hz) and 1,2-diequatorial vicinal coupling ($\varphi_{H-C-C-H}$ = 63°, $^3J_{H-H} \approx 3$ Hz) do not agree with the experimental values (coupling constants $J_{AA'}$ и $J_{BB'}$). The set of experimental values ($J_{AA'}$, $J_{AB'}$, $J_{A'B}$, $J_{BB'}$) corresponds to a fast two-positional exchange with one of the forms to be predominant (*ca.* 80–90% in the equilibrium mixture).

The $-CH_2CH_2-$ fragment of complexes **1** and **2** appears in the ^{1}H NMR spectra as an AA'BB' type spin system with sets of parameters which are practically the same as were found for the free ligand **L**. Therefore the complexation of the ligand **L** with $ZnCl_2$ or $CdCl_2$ does not affect the nature of the conformational exchange.

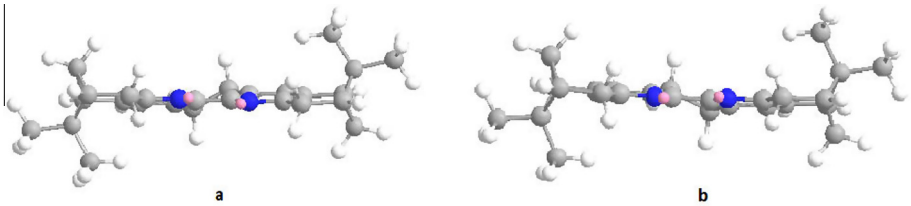

Scheme 3. Ligand **L** as *P*-helix (a) and *M*-helix (b).

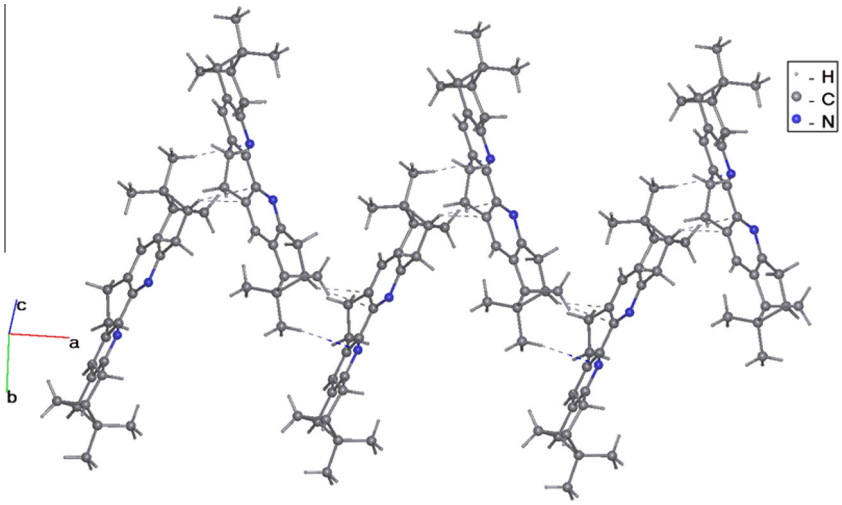

Fig. 2. Fragment of the 1D zigzag chains in the structure of **L**.

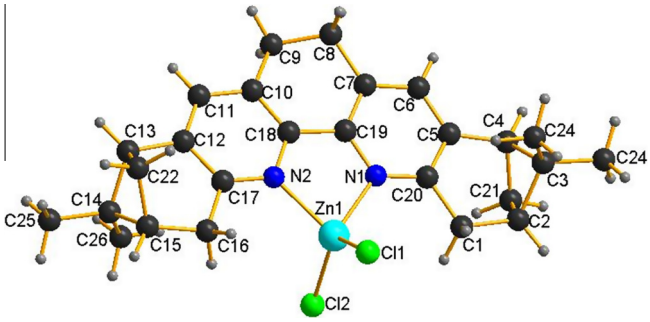

Fig. 3. Molecular structure of **1**.

Moreover, $^{13}C-^{1}H$ spin–spin couplings for complex **1** are in agreement with the presence of a spin system of the AA'BB' type for the–CH_2CH_2– fragment.

The dihydrophenanthroline fragment in the *P* or *L* helix form is an inherently dissymmetric chromophore, so the *P* and *L* helices should give opposite contributions to the total optical activity of the ligand **L** and its complexes. The experimentally determined optical rotations of complexes **1** and **2** are similar to that of the free ligand **L**. Quantum chemical calculations of optical activity ([α]) of the free ligand **L** or for the ligand **L** solvated by different solvents predict that the solvents do not significantly affect the strength of the rotation, although the exact values may differ (Fig. 1). Therefore, the observed pattern of optical activity is mainly due to the configuration of the molecules of **L** and complexes **1** and **2**, and the contribution of the solvent is less important. The experimental values of [α] fit well to the calculated curves for the *P*-helix, but not for the *M*-helix (Figs. 1, S1 and S2). Thus, we can assume that in solution, the ligand **L**, complex **1** and the monomeric form of complex **2** exist predominantly in the conformation with the *P*-helicity of the dihydrophenanthroline fragment.

3.3. X-ray structures

3.3.1. Crystal structure of **L**

The molecular structure of the compound **L** is shown in Fig. S3. The geometric parameters of the molecule correspond to average values in range 3σ [47]. The pyridine cycles are planar. In the pinene fragments, the six-membered carbocycles have the "Y" conformation. The C4, C5, C20, C1, C2 and C13, C12, C17, C16, C15 atoms are nearly coplanar. The mean deviations from the least squares plane are 0.014 and 0.007 Å, respectively. The C3, C21, C14 and C22 atoms deviate from these planes by −1.073(3), 1.081(3) Å, 1.063(3) and −1.075(3) Å, respectively. The molecules of **L** are assembled in 1D zigzag chains due to weak CH···N hydrogen bonds (H…N 2.870 Å) between the N atom of the pyridine cycle and the methyl groups of the terpene fragments and due to short CH···C contacts (H…C 2.759 Å) between the C atoms of pyridine cycle and the CH groups of the six-membered pinene carbocycles of a neighboring molecule (Fig. 2).

3.3.2. Crystal structure of $[ZnLCl_2]$ (**1**)

The crystal structure of **1** is built from mononuclear $[ZnLCl_2]$ molecules (Fig. 3). The Zn^{2+} ion coordinates two N atoms of the bidentate chelating ligand **L** and two Cl atoms in *cis*-positions. The Cl_2N_2 polyhedron is a distorted tetrahedron, having a τ_4-value of 0.9 [48]. The five-membered chelating ZnN_2C_2 ring closes as a result of the ligand coordination. The moiety consisting of the chelate and five six-membered organic cycles without gem-methyl atoms have a virtually planar structure. An average deviation from the root-mean-square atomic plane of the cycles is 0.013(6) Å, the Zn atom is deflected by 0.139 (5) Å. The Cl(1) and Cl(2) atoms deviate from this plane by −1.663(7) and 2.126(7) Å, respectively, on different sides. The six-member terpene carbocycles have the "Y" conformation with a low distortion, without the gem-dimethyl fragments. The supramolecular 3D structure of **1** is governed by van der Waals interactions and weak H bonds only. Packing of the molecules of **1** show CH…Cl contacts (H…Cl 2.84–2.86 Å) between the Cl atoms and the CH groups of the terpene fragments (Fig. S4a and b).

3.3.3. Crystal structure of $[Cd_2L_2Cl_4]$ (**2**)

The crystal structure of **2** consists of acentric molecules of the dinuclear complex $[Cd_2L_2Cl_4]$ (Fig. 4). According to the τ_5-values of 0.41 and 0.48 for the Cd(1) and Cd(2) atoms, respectively, the Cl_3N_2 polyhedron is an intermediate form between rectangular pyramid and trigonal bipyramid [49], with the two N atoms of the bidentate chelating ligand **L** and two bridging Cl atoms in the base. The Cd–Cl distances are 2.569(1) Å in the base (Table S4). The terminal Cl(1) and Cl(4) atoms occupy the axial pyramid vertices at shorter distances. Two Cl_3N_2 polyhedra share the Cl(2)…Cl(3) edge with distance of 3.418(2) Å. In the molecule, there are two five-membered chelate CdN_2C_2 rings and a Cd_2Cl_2 metallocycle. The Cd_2Cl_2 unit is planar. The average deviation from the

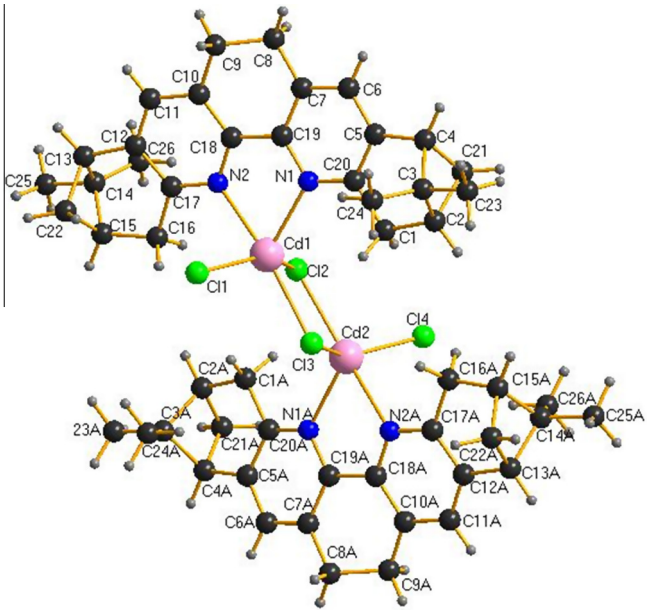

Fig. 4. Molecular structure of **2**.

root-mean-square atomic plane of the cycle is 0.032(1) Å. In the dinuclear Cd_2Cl_2 unit the Cd...Cd separation is 3.888(3) Å and the Cd–Cl–Cd angles are 98.3° and 96.4°. The terminal Cl(1) and Cl(4) atoms are situated in *trans*-positions relative to the dinuclear Cd_2Cl_2 unit. The six-membered terpene carbocycles of complex **2** have the "Y" conformation with a slight distortion with respect to the gem-dimethyl fragments. The molecules of the dinuclear complex **2** are assembled in 1D linear double chains due to two CH...Cl contacts between the Cl atom and CH groups of the pyridine cycle and six-membered carbocycle of the dihydrophenantroline fragment (H...Cl 2.76–2.77 Å) and due to CH...Cl contacts between the Cl atoms and the CH groups of the pyridine cycle (H...Cl 2.86 Å) of a neighboring molecule (Fig. S5a and b).

3.3.4. General remarks

According to the X-ray data, the dihydrophenanthroline fragments of **L** and **1** have a *P*-helix conformation in the solid state. The N2–C18–C19–N1 torsion angle is 12.1° in **L**, and this angle is 4.6° in **1**. In the solid state the dinuclear complex **2** is an asymmetric dimer, $[Cd_2Cl_4L^PL^M]$, where L^P is the ligand with the *P*-helix conformation for the dihydrophenanthroline fragment (in Fig. 4, the atoms of this fragment are labeled with the letters A) (NA2–CA18–CA19–NA1 = 13.1°), and L^M is the ligand with the *M*-helix conformation for the dihydrophenanthroline fragment (N2–C18–C19–N1 = −9.6°).

3.4. IR spectra

Bands at 1601, 1562 and 1547 cm^{-1} are observed in the IR spectrum of compound **L**, in the range for valence-bending vibrations of heterocycles. The positions of these bands are shifted to higher frequencies in the spectra of complexes **1** and **2** (1613, 1591, 1574 and 1577, 1561 cm^{-1} respectively). These shifts of the bands indicate the coordination of the N atoms of the ligand **L** to the metal ions. The far-IR spectra of complexes **1** and **2** exhibit bands for the stretching vibrations of the M–N bonds at 286 and 225 cm^{-1}. These observations are consistent with the coordination of the N atoms of the **L** molecules. A split *ν*(Zn–Cl) band with intensive maxima at 332 and 315 $cm^{-1}$is observed in the IR spectrum of the mononuclear complex **1**. The IR spectrum of complex **2** exhibits two split intensive bands at 266, 248 and 179, 168 cm^{-1} which can be attributed to stretching vibrations of the terminal and bridging Cd–Cl bonds, respectively. The far-IR spectra of **1** and **2** are similar to the spectra of Zn and Cd complexes having analogous structures [33].

3.5. Luminescence of the free ligand L and complexes 1 and 2 in solution and in the solid state

Fig. 5 shows the optical spectra of the ligand **L** and complexes **1** and **2** in CH_3CN. The absorption of the complexes is determined mainly by the ligand **L**, however, the incorporation of **L** into the coordination spheres of the Zn^{2+} and Cd^{2+} ions leads to a noticeable red shift of the absorption bands by 20 nm. This shift demonstrates that complex **1** and the monomeric form of **2** are not dissociated in solution.

The excitation luminescence spectra for the free ligand **L** and complexes **1** and **2** in CH_3CN and $CHCl_3$ solutions coincide with the absorption spectra of these compounds. Fig. 6a shows the excitation and luminescence spectra for the free ligand **L** in CH_3CN solution. The kinetics of the luminescence in this case (Fig. 6b) is well fitted by a mono-exponential approximation with a time of 0.66 ns. The emission spectra and kinetics for complexes **1** and **2** in CH_3CN are presented in the Supporting Information (Figs. S6 and S7, respectively). The coordination of the ligand **L** with the Zn^{2+} and Cd^{2+} ions in CH_3CN leads to a red shift of the luminescence bands by 27 and 9 nm, respectively. The kinetics of luminescence of the complexes **1** and **2** in CH_3CN are also well fitted by the mono-exponential approximation with times of 1.61 and 0.67 ns, respectively. The luminescence lifetimes of **L** and complexes **1** and **2** in CH_3CN do not depend on the wavelength of registration along the spectrum (from the blue to red wings of the luminescence bands). Table 1 shows the quantum yields and kinetic parameters of the luminescence decay for the ligand **L** and complexes **1** and **2** in acetonitrile.

In the solid state the luminescence spectra and kinetics for all our compounds become more complex. Fig. 7 shows the excitation and luminescence spectra for the free ligand **L** in the solid state. The maxima of luminescence bands in this case are red shifted in comparison with those for spectra in CH_3CN solution by 70 nm (4620 cm^{-1}). The same red shift is observed for the maxima of excitation bands. The kinetics of luminescence in the solid state become more complicate and can be fitted satisfactorily only in a two or three exponential approximation.

$$I(t) = A_1 e^{-\frac{t}{\tau_1}} + A_2 e^{-\frac{t}{\tau_2}} + A_3 e^{-\frac{t}{\tau_3}} \quad (1)$$

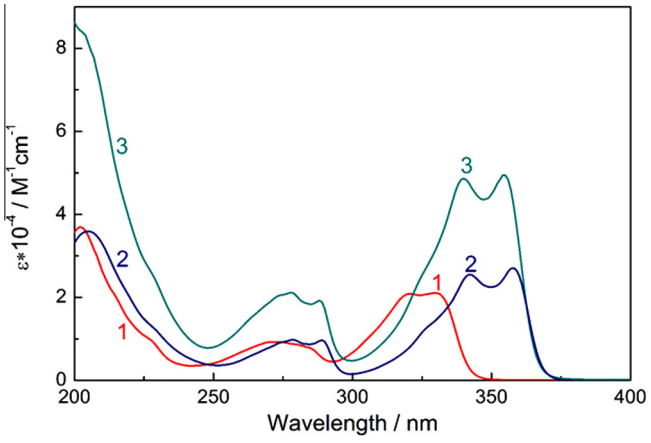

Fig. 5. The optical absorption (1, 2, 3) spectra of compounds **L**, **1** and monomeric form of **2** in CH_3CN.

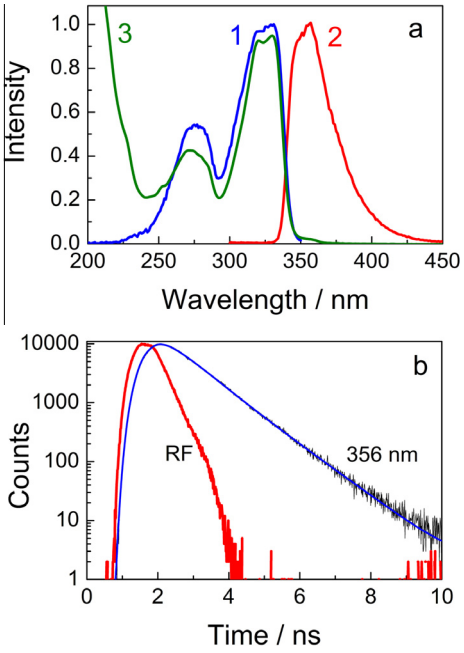

Fig. 6. The luminescence spectra (**a**) and kinetics (λ_{ex} = 300 nm, λ_{em} = 356 nm) (**b**) of the ligand **L** in acetonitrile. In (**a**) 1–3 – the excitation (λ_{em} = 356 nm), emission (λ_{ex} = 300 nm) and absorption spectra, respectively. RF in (**b**) – response function.

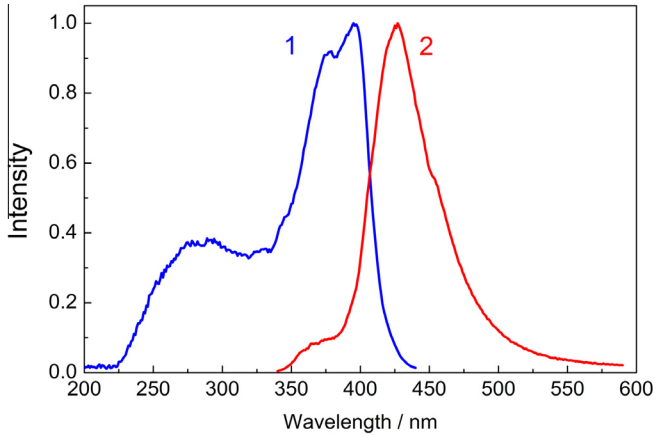

Fig. 7. The excitation (λ_{em} = 427 nm) (**1**) and luminescence (λ_{ex} = 300 nm) (**2**) spectra for the ligand **L** in the solid state.

At the maximum of the luminescence band (427 nm) for the ligand **L**, the kinetics are well described by two exponents with the times of 1.37 (95% of emitted photons in this exponent) and 4.73 (5%) ns. It should be also noted that the kinetics strongly depend on the wavelength of registration. On going along the luminescence spectrum from the blue to red region, the luminescence lifetimes (the times of exponents) significantly increase. For the ligand **L** this effect is shown in Fig. 8a, which demonstrates the significant difference of the kinetics at 427 and 575 nm. Furthermore, the use of an EPL-375 diode laser with a pulse duration of 60 ps allowed us to fix a negative A_1 amplitude of the first fast exponent (Eq. (1)) with a lifetime of 196 ps at 575 nm (Fig. 8b) for the ligand **L** in the solid state. The negative amplitude (the leading edge of the luminescence appearance) means that a substantial portion of luminescence at 575 nm occurs with a delay caused by the migration of excitation and a subsequent light emission at the centres with more low-lying energy levels. The decay of luminescence at 575 nm is described also by two exponents with times of 2.3 (63%) and 6.8 (37%) ns

The luminescence bands of complex **1** in the solid state are red shifted in comparison with those in CH_3CN solution by 21 nm (Fig. S8). In the center of the luminescence band (405 nm), the kinetics are described by two exponents with times of 0.33 (48%) and 1.38 (52%) ns (Fig. S9). On the far-red wing of the spectrum (600 nm), a rising edge of increasing luminescence intensity is seen with time of about 255 ps. The decay at this wavelength obeys a two exponential approximation with times of 2.02 (56%) and 6.03 (44%) ns. The same behavior of luminescence is observed for complex **2** (Figs. S10 and S11). In the blue range (415 nm) the decay of luminescence intensity occurs three times – 0.22 (7%), 1.17 (73%) and 2.16 (20%) ns (Fig. S11). At the red position (600 nm) the rise time is about 543 ps and the decay times are 3.01 (57%) and 7.91 (43%) ns. Table 1 presents the data of the luminescence of the ligand **L** and the complexes in the solid state.

This behavior of the luminescence kinetics of the free ligand **L** and the complexes in the solid state is not unusual. For example, the red shift of the luminescence band on going from solution to the solid state and the increase of the decay time in the red wing of the luminescence band were observed for anthracene [50]. Furthermore, in the solid state the luminescence kinetics of anthracene is also complicated (it can be fitted using three exponents) and depends on the registration wavelength. On going from 425 to 500 nm, the lifetimes of the exponents increase and at 600 nm the A_1 amplitude of the first exponent becomes negative with a duration of 1.4 ns. For anthracene, as well as for our compounds, this time is the duration which is required for an excitation to reach the molecules located near the "defect" centres. The same lifetimes were detected in Ref. [50] for thin films of solid anthracene deposited in a vacuum on quartz glass.

The luminescence quantum yields of the free ligand **L** and the complexes in the solid state have been determined relative to the quantum yield of anthracene in the polycrystalline state, which has quantum yield close to unity (0.93) [51]. The sharp decrease of the quantum yield of complex **1** in the solid state (Table 1) can be associated with the increased rate constants of non-radiative

Table 1
The maxima of the luminescence bands (λ_{max}/nm), the wavelengths of the recording of luminescence kinetics (λ_{reg}/nm), quantum yields (φ_f), lifetimes (τ_i/ns) and amplitudes (A_i) the processing of kinetics in two or three exponential approximation for compounds **L**, **1** and **2** in CH_3CN and in the solid state.

Compound	Condition	φ_f	λ_{max}	λ_{reg}	A_1	τ_1	A_2	τ_2	A_3	τ_3
L	CH_3CN	0.53	357	357	1	0.66				
	Solid	0.44	427	427	1	1.37	0.015	4.73		
				575	−0.091	0.196	1	2.3	0.201	6.79
1	CH_3CN	0.74	384	384	1	1.61				
	Solid	0.06	405	405	1	0.33	0.255	1.38		
				600	−0.191	0.235	1	2.02	0.268	6.03
2	CH_3CN	0.33	366	380	1	0.67				
	Solid	0.24	415	415	0.224	0.37	1	1.32		
				600	−0.187	0.543	1	3.01	0.293	7.91

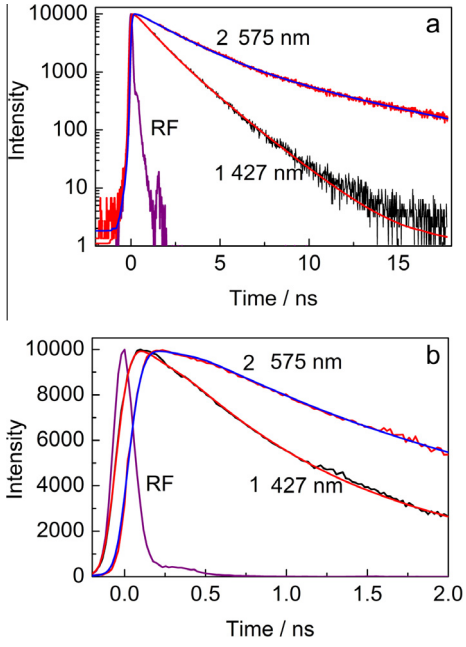

Fig. 8. The luminescence kinetics at 427 (**1**) and 575 (**2**) nm (λ_{ex} = 375 nm) for the ligand **L** in the solid state (**a**) and (**b**) the kinetics for 20 and 2 ns time intervals, respectively. RF – response function.

transitions, either to the ground state (S_0) or to the first triplet state (T_1). The same reasons can lead to a decrease of the quantum yields for the ligand **L** and complex **2** in the solid state, although to a lesser degree as compared with complex **1**.

4. Conclusions

For the first time, the synthesis and photophysical properties of luminescent zinc(II) and cadmium(II) complexes with a pentacyclic N-heterocycle containing two (–)-α-pinene fragments are reported. The complexes [$ZnLCl_2$] (**1**) and [$Cd_2L_2Cl_4$] (**2**), where **L** is (2*R*,4*R*,9*R*,11*R*)-3,3,10,10-tetramethyl-1,2,3,4,6,7,9,10,11,12-hexahydro-2,4,9,11-dimethanobenzo[*b,j*][1,10]phenanthroline, were obtained. Complex **1** is a mononuclear compound with the distorted tetrahedral structure of the Cl_2N_2 polyhedron, while **2** is a dinuclear complex with the distorted tetragonal pyramidal coordination polyhedron Cl_3N_2.

The *P*-helix conformation of the dihydrophenanthroline fragment of **L** is found in the crystal structure of **L** and in the structure of complex **1**. For the dinuclear complex **2**, one **L** molecule has the *P*-helix conformation for the dihydrophenanthroline fragment, whereas the other **L** molecule has the *M*-helix conformation of this fragment. The specific rotation [α] for the optimized structures of the compounds was determined by DFT calculations. An NMR study shows that the ligand **L**, complex **1** and the monomeric form of complex **2** in $CDCl_3$ solution show mainly the *P*-helix conformation of the dihydrophenanthroline fragment.

A full set of photophysical parameters for the free ligand **L** and complexes **1** and **2** was determined. The free ligand **L** displays bright blue luminescence (λ_{max} = 427 nm in solid state). The quantum yield of **L** is 44%. The coordination of the ligand **L** with Zn^{2+} and Cd^{2+}ions leads to a blue shift of the luminescence bands by 21 and 9 nm, respectively. In the solid state both complexes have a lower quantum yield compared with the free ligand **L**, however, their quantum yields are about an order of magnitude higher than the quantum yields of Zn(II) and Cd(II) complexes with a pyridophenazine ligand derived from chiral pinopyridine [33]. The quantum yield of dinuclear complex **2** is 24%. For the solid samples the excitation and luminescence spectra are significantly red-shifted as compared with the spectra in solution. The luminescence kinetics in the solid state for all the compounds is non-exponential and they depend on the wavelength of registration. On moving along the luminescence spectra to the red side, the decay times increase, and in the deep red region a rise in luminescence with times of 200–500 ps is observed. These processes are explained by the migration of excitation and the capture of excitation by molecules with low energy levels located close to "defective" centres in the crystal lattice.

Acknowledgements

The authors thank A.P. Zubareva and O.S. Koshcheeva for the supplied elemental analysis data and V.P. Fadeeva for the vapor-phase osmometry data. This work was financially supported by the Russian Foundation for Basic Research – Russia (Grants 14-03-00692, 15-03-03828), and Program of joint laboratories of NSU (Laboratory of Molecular Photonics).

Appendix A. Supplementary data

CCDC 1452329, 1452368 and 1452369 contains the supplementary crystallographic data for **1** and **2**. These data can be obtained free of charge via http://www.ccdc.cam.ac.uk/conts/retrieving.html, or from the Cambridge Crystallographic Data Centre, 12 Union Road, Cambridge CB2 1EZ, UK; fax: (+44) 1223 336 033; or e-mail: deposit@ccdc.cam.ac.uk. Supplementary data associated with this article can be found, in the online version, at http://dx.doi.org/10.1016/j.poly.2016.06.018.

References

[1] A. von Zelewsky, O. Mamula, J. Chem. Soc., Dalton Trans. (2000) 219.
[2] O. Mamula, A. von Zelewsky, Coord. Chem. Rev. 242 (2003) 87.
[3] M. Lama, O. Mamula, G.S. Kottas, L. De Cola, H. Stoeckli-Evans, S. Shova, Inorg. Chem. 47 (2008) 8000.
[4] H.-L. Kwong, H.-L. Yeung, C.-S. Yeung, W.-S. Lee, C.-S. Lee, W.-L. Wong, Coord. Chem. Rev. 251 (2007) 2188.
[5] J. Rich, M. Rodríguez, I. Romero, L. Vaquer, X. Sala, A. Llobet, M. Corbella, M.-N. Collomb, X. Fontrodona, Dalton Trans. 38 (2009) 8117.
[6] (a) H. Amouri, M. Gruselle, Chirality in Transition Metal Chemistry: Molecules, Supramolecular Assemblies and Materials, J. Wiley & Sons, Chichester, 2008; (b) A. von Zelewsky, Stereochemistry of Coordination Compounds, J. Wiley & Sons, Chichester, 1996.
[7] G. Muller, Dalton Trans. 44 (2009) 9692.
[8] T. Wu, C.-H. Li, Y.-Z. Li, Z.-G. Zhang, X.-Z. You, Dalton Trans. 39 (2010) 3227.
[9] S.G. Telfer, G. Bernardinelli, A.F. Williams, Dalton Trans. (2003) 435.
[10] A.V. Tkachev, Mendeleev Chem. J. 42 (1998) 42.
[11] S.V. Larionov, A.V. Tkachev, Mendeleev Chem. J. 48 (2004) 154.
[12] S.V. Larionov, Russ. J. Coord. Chem. 38 (2012) 1.
[13] P. Hayoz, A. Von Zelewsky, Tetrahedron Lett. 33 (1992) 5165.
[14] G. Chelucci, G. Logira, G. Murineddu, G.A. Pinna, Tetrahedron Lett. 43 (2002) 3601.
[15] S.A. Popov, M.M. Shakirov, A.V. Tkachev, N. De Kimpe, Tetrahedron 53 (1997) 17735.
[16] S.V. Larionov, Z.A. Savel'eva, R.F. Klevtsova, L.A. Glinskaya, E.M. Uskov, M.I. Rakhmanova, S.A. Popov, A.V. Tkachev, J. Struct. Chem. 52 (2011) 531.
[17] S.V. Larionov, Z.A. Savel'eva, R.F. Klevtsova, E.M. Uskov, L.A. Glinskaya, S.A. Popov, A.V. Tkachev, Russ. J. Coord. Chem. 37 (2011) 1.
[18] G. Muller, J.-C.G. Bünzli, J.P. Riehl, J.P. Suhr, A. von Zelewsky, H. Mürneret, Chem. Commun. (2002) 1522.
[19] J. Liu, X.-P. Zhang, T. Wu, B.-B. Ma, T.-W. Wang, C.-H. Li, Y.-Z. Li, X.-Z. You, Inorg. Chem. 51 (2012) 8649.
[20] L. Yang, A. von Zelewsky, H.P. Nguyen, G. Muller, G. Labat, H. Stoeckli-Evans, Inorg. Chim. Acta 362 (2009) 3853.
[21] A.P. de Silva, H.Q.N. Gunaratne, T. Gunnlaugsson, A.J.M. Huxley, C.P. McCoy, J.T. Rademacher, T.E. Rice, Chem. Rev. 97 (1997) 1515.
[22] N.C. Lim, H.C. Freake, C. Brückner, Chem. Eur. J. 11 (2005) 38.
[23] W. Yang, H. Schmider, Q. Wu, Y. Zhang, S. Wang, Inorg. Chem. 39 (2000) 2397.
[24] T. Sano, Y. Nishio, Y. Hamada, H. Takahashi, T. Usuki, K. Shibata, J. Mater. Chem. 10 (2000) 157.
[25] G. Yu, S. Yin, Y. Liu, Z. Shuai, D. Zhu, J. Am. Chem. Soc. 125 (2003) 14816.
[26] E. Kimura, T. Koike, Chem. Soc. Rev. 27 (1998) 179.

[27] N.J. Williams, W. Gan, J.H. Reibenspies, R.D. Hancock, Inorg. Chem. 48 (2009) 1407.
[28] A.W. Czarnik, Acc. Chem. Res. 27 (1994) 302.
[29] B. Valeur, I. Leray, Coord. Chem. Rev. 205 (2000) 3.
[30] X. Liu, A. González-Castro, I. Mutikainen, A. Pevec, S.J. Teat, P. Gamez, J.S. Costa, E. Bouwman, J. Reedijk, Polyhedron 110 (2016) 100.
[31] G.A. Ardizzoia, S. Brenna, S. Durini, B. Therrien, Polyhedron 90 (2015) 214.
[32] B.M. Momeni, S. Heydari, Polyhedron 97 (2015) 94.
[33] S.V. Larionov, T.E. Kokina, V.F. Plyusnin, L.A. Glinskaya, A.V. Tkachev, Y.A. Bryleva, N.V. Kuratieva, M.I. Rakhmanova, E.S. Vasilyev, Polyhedron 77 (2014) 75.
[34] E.S. Vasilyev, A.M. Agafontsev, A.V. Tkachev, Synth. Commun. 44 (2014) 1817.
[35] T. Wu, X.-Z. You, P. Bouř, Coord. Chem. Rev. 284 (2015) 1.
[36] S. Goswami, K. Aich, S. Das, C. Das Mukhopadhyay, D. Sarkar, T.K. Mondal, Dalton Trans. 44 (2015) 5763.
[37] J.B. Foresman, T.A. Keith, K.B. Wiberg, J. Snoonian, M.J. Frisch, J. Phys. Chem. 100 (1996) 16098.
[38] Dalton, a molecular electronic structure program, Release Dalton 2015.0, 2015, see http://daltonprogram.org.
[39] K. Aidas, C. Angeli, K.L. Bak, V. Bakken, R. Bast, L. Boman, O. Christiansen, R. Cimiraglia, S. Coriani, P. Dahle, E.K. Dalskov, U. Ekström, T. Enevoldsen, J.J. Eriksen, P. Ettenhuber, B. Fernández, L. Ferrighi, H. Fliegl, L. Frediani, K. Hald, A. Halkier, C. Hättig, H. Heiberg, T. Helgaker, A.C. Hennum, H. Hettema, E. Hjertenæs, S. Høst, I.-M. Høyvik, M.F. Iozzi, B. Jansik, H.J.Aa. Jensen, D. Jonsson, P. Jørgensen, J. Kauczor, S. Kirpekar, T. Kjærgaard, W. Klopper, S. Knecht, R. Kobayashi, H. Koch, J. Kongsted, A. Krapp, K. Kristensen, A. Ligabue, O.B. Lutnæs, J.I. Melo, K.V. Mikkelsen, R.H. Myhre, C. Neiss, C.B. Nielsen, P. Norman, J. Olsen, J.M.H. Olsen, A. Osted, M.J. Packer, F. Pawlowski, T.B. Pedersen, P.F. Provasi, S. Reine, Z. Rinkevicius, T.A. Ruden, K. Ruud, V. Rybkin, P. Salek, C.C.M. Samson, A. Sánchez de Merás, T. Saue, S.P.A. Sauer, B. Schimmelpfennig, K. Sneskov, A.H. Steindal, K.O. Sylvester-Hvid, P.R. Taylor, A.M. Teale, E.I. Tellgren, D.P. Tew, A.J. Thorvaldsen, L. Thøgersen, O. Vahtras, M.A. Watson, D.J.D. Wilson, M. Ziolkowski, H. Ågren, The Dalton quantum chemistry program system, WIREs Comput. Mol. Sci. 4 (2014) 269.
[40] F. Neese, WIREs Comput. Mol. Sci. 2 (2012) 73.
[41] A.A. Bothner-By, Adv. Magn. Reson. 1 (1965) 195.
[42] (a) A.L. Spek, PLATON, A Multipurpose Crystallographic Tool, version 10M, Utrecht University, The Netherlands, 2003;
(b) A.L. Spek, J. Appl. Crystallogr. 36 (2003) 7.
[43] F. Macrae, P.R. Edgington, P. McCabe, E. Pidcock, G.P. Shields, R. Taylor, M. Towler, J. van de Stree, J. Appl. Crystallogr. 39 (2006) 453.
[44] G.M. Sheldrick, SHELX-97, Programs for Crystal Structure Analysis (Release 97–2), University of Göttingen, Germany, 1997.
[45] G.M. Sheldrick, SADABS Version 2.01, Bruker AXS Inc., Madison, Wisconsin, USA, 2004.
[46] O.V. Shishkin, J. Struct. Chem. 41 (2000) 383.
[47] F.H. Allen, O. Kenard, D.G. Watson, L. Bramer, A.G. Orpen, R. Taylor, J. Chem. Soc., Perkin Trans. II (1987) S1.
[48] L. Yang, D.R. Powell, R.P. Houser, Dalton Trans. 9 (2007) 955.
[49] A.W. Addison, T.N. Rao, J. Chem. Soc., Dalton Trans. 7 (1984) 1349.
[50] T.-S. Ahn, A.M. Müller, R.O. Al-Kaysi, F.C. Spano, J.E. Norton, D. Beljonne, J.-L. Brédas, C.J. Bardeen, J. Chem. Phys. 128 (2008) 054505.
[51] G.T. Wright, Proc. Phys. Soc. B 69 (1955) 241.